Scanning-tunneling-microscopy and photoemission study of an alkali-metal-induced structural phase transition: Si(111)-(7×7) into Si(111)-Na(3×1)

J. J. Paggel, G. Neuhold, H. Haak, and K. Horn
Fritz-Haber-Institut der Max-Planck-Gesellschaft, Faradayweg 4-6, 14195 Berlin, Germany
(Received 24 March 1995)

The structural phase transition from the clean Si(111)-(7×7) reconstruction to the Na-stabilized (3×1) reconstruction of this surface is studied using scanning tunneling microscopy as well as core- and valence-level photoemission. By combining the laterally integrating technique of photoemission with the highly spatially resolving technique of scanning tunneling microscopy, the kinetics of the phase transition is explained on an atomic scale. In addition to the information on the kinetic pathway of the phase transition, we present a simple model of the dynamics, which explains the time dependence of the transition rate from the (7×7) to the Na(3×1) reconstruction of the Si(111) surface. It is demonstrated that samples can be prepared with both surface reconstructions coexisting on the surface in any desired ratio. These coexisting islands show the properties of the pure reconstructions, which demonstrates a strong lateral modulation of the position of the Fermi level in the semiconductor band gap at the surface.

I. INTRODUCTION

The interaction of metals with semiconductor surfaces is a topic that has been discussed for more than a hundred years in the scientific literature.[1] However, the evolution of the metal-to-semiconductor contact as a function of overlayer thickness is still not completely understood in detail, in spite of the technological interest (e.g., contacts to semiconductor devices), as well as from the point of view of basic research (formation of interface states and band alignment). Adsorption of simple metals, such as the alkali metals, has significance as a model system for the adsorption of atoms on solid surfaces in general.[2] In order to arrive at a model system for metal-semiconductor contacts, the combination of the most intensely studied semiconductor surface, Si(111)-(7×7), with sodium atoms, which do not diffuse into silicon at room temperature, is a natural choice. This material combination shows a very interesting behavior: it has been reported by Daimon and Ino[3] that all alkali metals are capable of changing the (7×7) reconstruction into an alkali-metal-stabilized (3×1) reconstruction. For the case of Na on Si(111)-(7×7), it has been shown that the (7×7)→Na(3×1) transition takes place at a temperature which is higher than the desorption temperature of Na on the Si(111)-(7×7) surface.[4] Tikhov and co-workers[4] have demonstrated, using temperature-programmed desorption (TPD) experiments, that this Si(111)-Na(3×1) surface is less susceptible to oxidation than the bare surface, which is surprising since alkali-metal adsorption on semiconductor surfaces usually promotes oxidation.[5] Following these initial studies, a number of authors have investigated the nature of this metal-induced reconstruction of a semiconductor surface. Jeon and co-workers[6,7] used the scanning-tunneling-microscopy (STM) technique and demonstrated the presence of double row structures showing a (3×1) periodicity. The double row structure was initially assumed to consist of Na adatoms. Since the surface was found to be semiconducting by means of scanning tunneling spectroscopy, this structure was prosed to be a Mott-Hubbard insulator.[6] Following a careful calibration of the Na content of the surface by means of core-level photoemission and scanning tunneling microscopy, the double row structure was assigned to Si atoms.[8,9] The controversy of the assignment of the double rows seems now to have been settled[10–12] in favor of Si atoms, and this also seems to be the case for several other metal-induced reconstructions of the Si(111) surface.[10,11] The alkali-metal coverage in the 3×1 reconstruction of the Si(111) surface is one Na atom per 3×1-unit cell and the semiconducting character of the surface is easily explained in the single-electron picture. Even though the nature of the Na(3×1) reconstruction is now understood, there are still a number of open issues: the position of the alkali-metal atom in the surface reconstruction is not known. It is certainly not difficult to propose a model for this surface reconstruction, which satisfies the known boundary conditions of symmetry and Na coverage as done by Weitering *et al.*,[12] but up to now, no data being sensitive to the positions of the ion cores in the surface reconstruction have been published, while the CaF-induced Si(111)-(3×1) reconstruction has recently been investigated using surface x-ray scattering.[13] Another problem to be discussed is the kinetic pathway of the transition from the (7×7) to the Na(3×1) reconstruction, while the kinetics of the transition from the Na(3×1) reconstruction to the clean 7×7 reconstruction has been the subject of a recent high-temperature scanning-tunneling-microscopy study.[14] Here, we present a STM and photoemission study of the structural phase transition from the (7×7) to the Na(3×1) reconstruction of the Si(111) surface, where the morphology of the coexistence of the two phases, as well as its electronic structure is investigated. Using the combination of the two techniques, a kinetic model for the phase transition is given.

0163-1829/95/52(8)/5813(11)/$06.00

II. EXPERIMENT

Photoemission experiments were carried out at the BESSY (Berliner Speicherringgesellschaft für Synchrotronstrahlung mbH) wiggler/undulator beam line TGM6, using a photon energy of 122 eV at a resolution of 300 meV for spectroscopy of the Si $2p$ core level and at a photon energy of 76 eV at a resolution of 170 meV for spectroscopy of the Na $2p$ core level and the valence-band region. The vacuum system was equipped with a turbomolecular pump, an ion getter pump, and a titanium sublimator pump, resulting in a base pressure of below 5×10^{-11} mbar. The electron energy analyzer was an angle-resolving hemispherical analyzer HA50 (VSW) with 50-mm mean radius (angular acceptance 1.5°). Additional equipment at this vacuum system was low-energy electron-diffraction (LEED) optics, a commercial Kelvin probe ($\Delta\Phi$) for measurement of the alkali-metal-induced work-function change, and a load lock for sample transfer. Scanning-tunneling-microscopy (STM) experiments were carried out in a different vacuum system, similarly equipped as the photoemission system. The STM used for these experiments was home-built and based on a commercial Nanoscope II (Digital Instruments Inc.) electronics.[8] The base pressure in this system was below 1×10^{-10} mbar. In both vacuum systems Na was evaporated from commercial SAES-getter sources that were carefully degassed. The rise in pressure during evaporation was always below 1×10^{-10} mbar and mainly due to the Na itself as checked by using a mass spectrometer. Si samples were p doped (boron, 5–10 Ω cm, Wacker Chemitronic GmbH) and n-doped (phosphorus, 5–10 Ω cm, Wacker Chemitronic GmbH). The p-doped samples were oriented better than 0.5° with respect to the {111} direction as checked directly using the STM. The n-doped samples were 3°–4° misoriented in the $[\bar{2}11]$ azimuth. All STM images presented here are taken from p-doped samples, that were misoriented by 0.5° in the $[\bar{2}11]$ azimuth. The Si(111)-(7×7) reconstruction was proposed using the careful degassing technique proposed by Swartzentruber *et al.*,[15] resulting in defect densities of far less than $\frac{1}{100}$th of a monolayer as demonstrated by our STM images. Sample heating was accomplished using direct current heating. In order to avoid interference between the direction of the heating current and the step structure of the surface,[16] the current was passed along the $[01\bar{1}]$ direction, i.e., parallel to the direction of the step edges. The Si(111)-Na(3×1) is prepared using the procedure described by Tikhov, Surnev, and Kiskinova:[4] Na was evaporated onto the clean Si(111)-(7×7) surface, which is held at a temperature between 300 °C and 400 °C, while the Na flux was reduced as far as possible in order to prepare mixed phases of the (7×7) and the Na(3×1) reconstruction in a controlled manner by shutting off the Na flux at the desired Na(3×1) coverage Unless stated otherwise, all samples were annealed after preparation for about 30 s in order to improve the quality of the Na(3×1) reconstruction. By calibrating the Na flux in a parallel experiment on the adsorption of Na on the Si(111)-(7×7) reconstruction at room temperature,[9] we were able to determine the minimum dose of Na atoms necessary to convert the surface reconstruction from (7×7) to Na(3×1) being approximately 2–3 ML, where 1 ML is defined as one adatom per Si atom in the topmost layer of the bulk-terminated (1×1) surface. Using this definition of 1 ML, the Na coverage in the Na(3×1) reconstruction is thus $\frac{1}{3}$ ML. As will be shown later on, the misorientation of the substrate has a strong influence on the formation of the Na(3×1) reconstruction, therefore the necessary flux to prepare a Si(111)-Na(3×1) reconstruction might depend on the miscut angle of the surface.

All data presented in this paper were taken from surfaces that were prepared with the ion gauge in the vacuum system switched off and checked with LEED *after* data acquisition, since it turned out that the photoemission spectra from the Na $2p$ core level were seriously altered after the use of LEED, even though this was well degassed (pressure increase lower than 1×10^{-10} mbar). A second observation is that the Fermi level of the Si(111)-Na(3×1) reconstruction, which is semiconducting and unpinned in the clean state, is pinned within less than 60 min of surface preparation, at a position close to midgap at base pressures in the upper 10^{-11} mbar range. This pinning of the Fermi level might be responsible for the broad range of the reported Na-induced work-function change relative to the Si(111)-(7×7) reconstruction.[7,8,12] Surfaces that were investigated with LEED prior to the photoemission experiment were always found to be pinned.

In order to study different stages of conversion of the Si(111)-(7×7) reconstruction into the Si(111)-Na(3×1) reconstruction, each stage of the phase transition from the (7×7) to the Na(3×1) reconstruction was prepared starting from a "reflashed" Si(111)-(7×7) reconstruction, i.e., all spectra and images are from samples that were unpinned.

III. RESULTS AND DISCUSSION

We start the discussion with scanning-tunneling-microscopy data, in order to discuss the morphology of the alkali-metal-induced phase transition, which will lead to a qualitative understanding of the phase transition and its kinetics. The photoemission data to be discussed later will provide deeper insight into the electronic structure of the coexistence of the two surface reconstructions, and will lead to a qualitative model for the kinetics of the transition from the (7×7) to the Na(3×1) reconstruction of the Si(111) surface.

However, before discussing the STM images, we have to comment on the graphic representation of our data. In order to highlight the step structure to be discussed in Figs. 1 and 2, the images are shown in a pseudo-light-shading representation. In order to demonstrate the effect of this data manipulation, the bottom part of Fig. 1(a) is shown in the inset in the right top part of the same figure, but without data manipulation. The STM images in Figs. 2 and 3 were manipulated to show the atomic structure on different terraces using a single gray scale. The height difference in the image produced from the step edge exceeds the atomic modulation on the terrace

height by far. In order to enhance the atomic structure of the terraces, the imaged step height is artificially reduced in the images by 50%. This procedure has not been applied for the data used for Fig. 2(b), where the imaged step height is shown using a cross section of the imaged surface.

Figure 1 shows the step structure of (a) a typical (7×7) reconstructed surface, which exhibits only single-layer steps with mostly straight steps edges, and (b) the step structure of a surface partly converted to the Na(3×1) reconstruction. The large differences in the step structure between the two surface phases are quite surprising. Closer inspection of the atomic structure of this surface [Fig. 2(a)] demonstrates that the upper terrace of the trenches in the step edges is always (7×7) reconstructed, while the bottom of the trench is Na(3×1) reconstructed. By measuring the step heights as shown in Fig. 2(b), one finds that one clean surface single layer step height corresponding to *two* "step edges," leading from (7×7) to Na(3×1), and back to the (7×7). In other words, the single "step" on a mixed (7×7)-(3×1) surface has two functions: that of a step and that of a domain boundary. At the domain boundary, there are several influences on the difference in the apparent height of the two domains: (a) there is the geometrical height difference, resulting from the different surface reconstructions, and (b) there is a possible band offset between the two different domains, which might cause a difference in the tunneling probability and render a straightforward interpretation of the observed height differences difficult. A third, but less important, contribution is the difference in the work function of the two pure surface reconstructions, which amounts to 300 meV.[8] It is well known that the work function of a polycrystalline surface (or "polydomain surface) is the weighted mean value of the different surface orientations or domains. The mean value is adjusted through a lateral variation of the electrochemical potential, which leads to the building up of dipole fields at the domain boundaries.[17] This lateral variation of the electrochemical potential might give rise to a lateral variation of the tunneling probability and, therefore, influence the imaged step height. The work function change of the surface as function of the relative Na(3×1) coverage (not shown here) is well described within the experimental error using this simple concept. As a fourth contribution to the imaged height difference between the (7×7) and the Na(3×1) domains on the surface, a potential tip-induced band bending at the semiconducting Na(3×1) surface can occur. For example, the imaged step height from the (7×7) domains to the Na(3×1) domains in Fig. 3(a), turns out to be 2.5 Å instead of about 1.6 Å, as imaged in Fig. 2. Both images were obtained using different

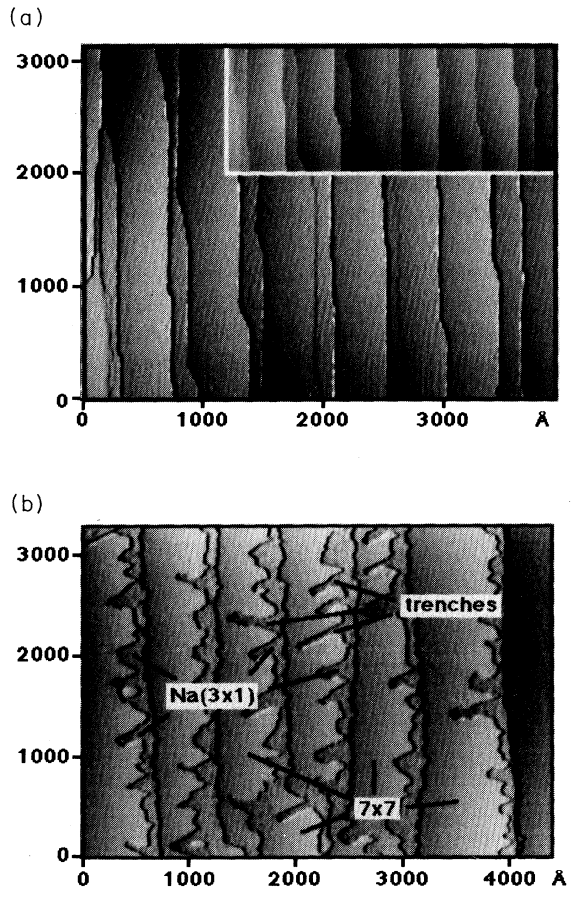

FIG. 1. Scanning-tunneling-microscopy images of (a) the clean Si(111)-(7×7) reconstructed surface with the typical straight step edges ($V_{bias}=1.5$ V, $I_t=900$ pA) and (b) the surface partially converted to the Na(3×1) reconstruction with "trenches" in the terraces extending into the terrace ($V_{bias}=1.8$ V, $I_t=1$ nA). The inset in (a) shows the bottom part of the image before picture processing. See text for details.

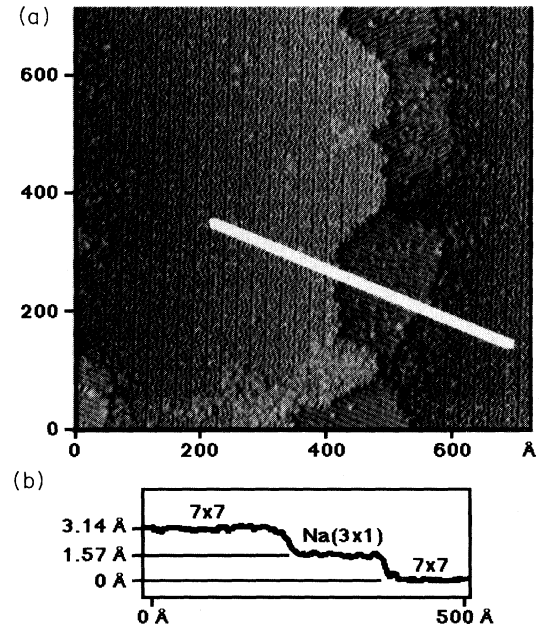

FIG. 2. Scanning-tunneling-microscopy image of the initial stage of the conversion of the (7×7) reconstruction into the Na(3×1) reconstructed surface with atomic resolution. Both types of domains do not show any sign of a lateral band bending across the terrace, which would be expected to result in a "bent terrace" ($V_{bias}=2.2$ V, $I_t=620$ pA).

tunneling conditions, i.e., bias voltage and tunneling current, even though the bias voltages used were very similar (2.0 and 2.2 V). This clearly demonstrates the difficulty of obtaining step heights and thus structural information from semiconductor surfaces possessing different local structures. A detailed study of the dependence of the imaged step height and the tunneling conditions has not been carried out as a function of Na(3×1) coverage. The Na(3×1) coverage of the surface influences the measured "band offset" between the two domains as will be demonstrated below. However, one feature that is simple to evaluate is the apparent step height as two domain boundaries are crossed, since in this situation, the two interface dipoles as well as all other effects mentioned above cancel exactly. Thus, the information that can be extracted from Fig. 2(b) is the layer-to-layer distance in the {111} direction of Si, which is always 3.14 Å.

Atomically resolved images of surfaces such as the one in Fig. 1(b), as shown in Fig. 2 also demonstrate that each single terrace is imaged with the same apparent height, while being modulated by the atomic corrugation of the terrace. There is no "bowing" of the terraces in the vicinity of the step edges, as one would expect for a laterally varying electrostatic potential across a terrace, i.e., the absolute height of the single terraces imaged by the STM tip (despite the atomic corrugation of the surface) does not depend on its position on the terrace. From the absence of this effect we can conclude that the interface dipole, which might be responsible for a variation of tip-sample separation, extends over only a few unit cells in the vicinity of the step edge. The details on the band alignment in this coexistence structure have to be deferred until the discussion of the Si 2*p* core-level spectra, since the analysis of band offsets is much more straightforward using core-level photoemission than in STM. However, even for very low coverages of the surface with the Na(3×1) reconstruction, there are always just the pure phases of the surface reconstruction visible in the STM image. There are no intermediate surface reconstructions or inhomogeneous terraces.

Figure 4 shows the step structure of a surface completely converted to the Na(3×1) reconstruction, where the same data manipulation as in Fig. 1 has been applied. In contrast to the surface morphology shown in Fig. 1, there are islands on the larger terraces, and fingerlike structure reaching over several hundred Å from the upper terraces onto the lower ones. Images with atomic resolution (not shown here) reveal that the entire surface is covered by the Na(3×1) reconstruction.[7,8] In order to

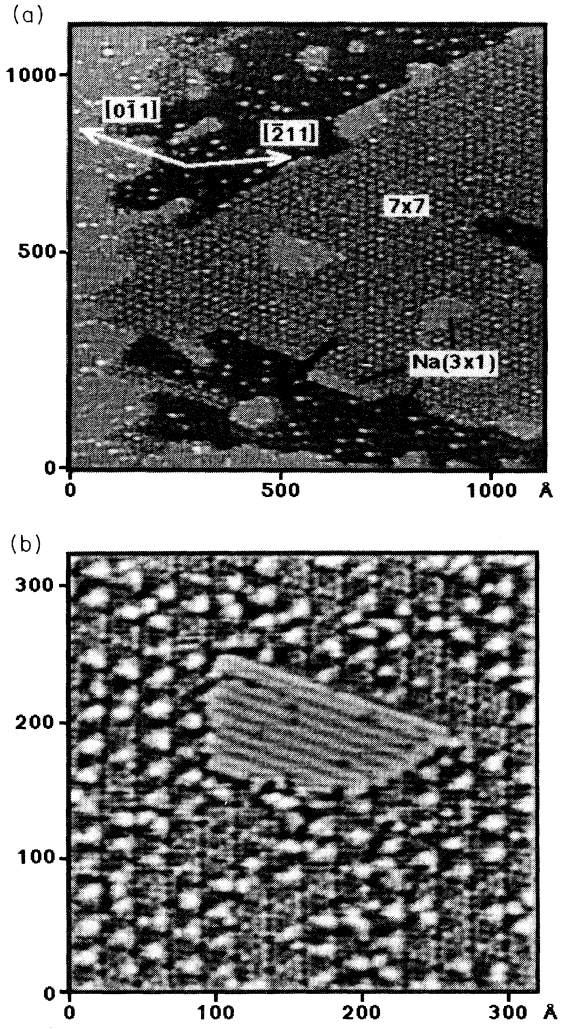

FIG. 3. (a) Large area scan of a nearly completely to the Na(3×1)-reconstruction converted surface ($V_{bias}=2.0$ V, $I_t=200$ pA). The large domain in the center of the image is (7×7) reconstructed, the surrounding domains are Na(3×1) reconstructed. For details see text. (b) Enlarged image of the island near the center of (a) on the (7×7) domain. The image shows the Na(3×1) reconstruction of the island, as well as the (7×7) reconstruction of the surrounding domain.

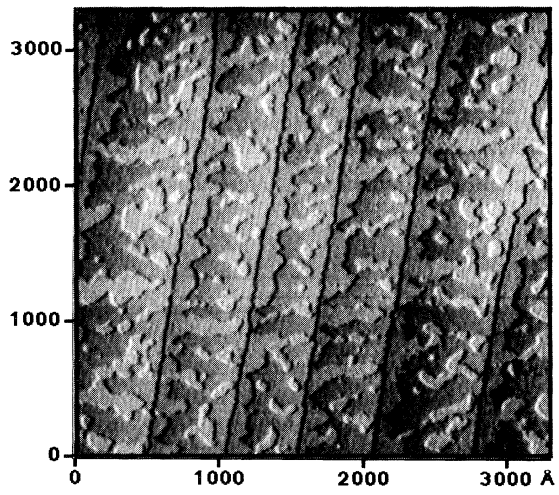

FIG. 4. STM image showing the step structure of a surface completely converted to the Na(3×1) reconstruction. All steps are 1 ML high. Note the existence of islands on larger terraces and the meandering step edges, which are never seen on the original (7×7)-reconstructed surface, which is the surface reconstruction used to prepare the Na(3×1) reconstruction on ($V_{bias}=1.5$ V, $I_t=460$ pA).

understand the kinetic pathway of the phase transition from the (7×7) to the Na(3×1) reconstruction, it is necessary to give an explanation for the appearance of the islands on the Na(3×1)-reconstructed surface. First of all, the islands originate from a large mass transport, which is obviously necessary to convert the (7×7) into the Na(3×1) reconstruction. This mass transport is already visible in the images of the initial stages of the phase transformation [Fig. 1(b)], where the step structures change drastically. The indication for the large mass transport is not the presence of the trenches in the terraces, but the changes in the step structure of the layer that forms the trenches, which is no longer as regular as the step edge of the original surface. Thus, there is mass transport out of the 7×7 reconstruction, which contains 104 atoms per (7×7) unit cell, while the bulk-terminated (7×7) unit cell contains 98 atoms.[18,19] However, mass transport cannot be the only reason for the appearance of the islands, since it should be energetically more favorable to produce a meandering step edge rather than to generate an islandlike structure in the center of a terrace.

In order to obtain information on this process, STM images of the phase transition in a range of coverages, where nearly the whole surface is converted to the Na(3×1) reconstruction were recorded and are shown in Fig. 3. Figure 3(a) shows a large scan of the surface, where an island of remaining (7×7) reconstruction exists, nearly completely surrounded by the Na(3×1) reconstruction. The overall appearance of the (7×7)-reconstructed island is triangular. The crystallographic directions on the surface are indicated in the image. These directions are determined by investigating of the surface reconstructions, and since the images are not drift corrected, the enclosed angle of the two arrows differs from the theoretical value of 150°. The (7×7) reconstructed domain already has some Na(3×1)-reconstructed islands on top, one of which is shown in Fig. 3(b) with higher magnification. The height difference between the Na(3×1) reconstruction on top of the (7×7) domain and the Na(3×1) domain surrounding the (7×7) domain is exactly the monolayer step height of Si(111). Figure 3(a) thus gives an important hint on the formation of the island structure of the Na(3×1) reconstruction: there are two contributions to the formation of the islands. First, there is the mass transport necessary to convert the (7×7) reconstruction into the Na(3×1) reconstruction, as discussed above. The second contribution is the kinetic pathway of the phase transition. There is a preferred growth direction of the Na(3×1) reconstruction along its double rows, which run along the $\langle 1\bar{1}0 \rangle$ direction of the substrate. However, the growth proceeds in the $\langle \bar{1}10 \rangle$ and the $\langle 1\bar{1}0 \rangle$ direction, as easily seen by the triangular shape of the remaining (7×7) domains and the formation of the trenches in the step edges in Fig. 1(b). If one of the two directions were preferred, only one orientation of the trenches relative to the step edge should be observed, and there should be no possibility to generate triangular-shaped remaining (7×7) domains on the surface. Combined with a slight misorientation of the surface of less than 0.5° in the direction of the $(\bar{2}11)$ azimuth, this eventually results in a pinching off of the (7×7) domains from the step edge, i.e., the trenches in the terraces consisting of the Na(3×1) reconstruction grow into the (7×7) domain until they reach the next step edge. If two Na(3×1)-reconstructed domains meet at this step edge, as shown in Fig. 3(a), a (7×7)-reconstructed island, surrounded by domains of Na(3×1) is generated. Keeping in mind that excess Si has to be removed from the (7×7) reconstruction to generate the Na(3×1) reconstruction, these additional atoms have to diffuse either on the (7×7) domains or on the Na(3×1) domains. The formation of the Na(3×1)-reconstructed islands on top of the remaining (7×7) domains clearly shows that this diffusion occurs on the 7×7 domains, where it occasionally leads to the formation of isolated Na(3×1) islands.

There is another effect which promotes the formation of the island structure: as soon as a Na(3×1) island is formed on the (7×7) domain, it is very stable and actually pins the domain boundary, as clearly demonstrated by the increased occurrence of Na(3×1) islands on the (7×7) domains at the boundaries to the Na(3×1) reconstruction. This process is demonstrated by the fact that Na(3×1) reconstructed islands, such as the one marked by an arrow in the lower left quadrant of Fig. 3(a), "shadow" a thinned (7×7) domain in the $[0\bar{1}1]$ direction (only two units cell wide actually) from the growth front from being obliterated, by keeping it from being attacked along the direction of the double rows. Growth of the Na(3×1) reconstruction perpendicular to its double row direction seems to be much slower than in the direction along these rows, if it occurs at all. We may thus conclude that the origin of the island structure of the Na(3×1) reconstruction is caused by (1) the mass transport *out of* the (7×7)-reconstructed ares, (2) the diffusion of excess Si *on top* of the (7×7) domains, and (3) the growth kinetics of the Na(3×1) domains, which have a *preferred growth direction.*

Another point to discuss on the basis of Fig. 3(b) is the information contained in the atomic resolution obtained on the (7×7) reconstructed domain in this image. This surface has been quenched after the preparation of the Na(3×1) reconstruction, which is the reason for the different appearance of this (7×7) domain, as compared to Fig. 2. However, to maintain the flow of argument, we will discuss this point later on and refer to Fig. 3(b) below.

Let us now examine the electronic structure of the two surfaces in the coexistence phase, by the use of core-level photoemission. Core-level photoemission can identify the different phases, because of the distinct signature of each phase, as can be seen from the top and the bottom spectrum of Fig. 5(a), where the spectrum of a Na induced (3×1) surface and the clean Si(111)-(7×7) surface are compared. It is obvious from the difference in shape, and even more so from the spectra of different mixtures of Na(3×1)/(7×7) reconstructions, which are indicated as percentages of Na(3×1) phase, that a distinction can be readily achieved. These data were recorded at a photon energy of 122 eV, corresponding to a kinetic energy of 17 eV, which is a balance between surface and bulk sensitivity. Binding energies are referred to the Fermi level E_F,

which was determined from the spectrum of a copper plate in electrical contact with the sample. The percentages of (3×1) structure were evaluated from the result of a line-shape analysis, which is shown beneath the top and bottom spectra. The Na(3×1) spectrum consists of one bulk and two surface emission lines, marked *b* and *S*1/*S*2, respectively.[8] The spectrum of the (7×7) surface is also represented by one bulk and two surface lines. We have recently shown in a high-resolution study that the Si 2*p* spectrum of the (7×7) spectrum is actually made up of four different surface components[20] instead of the two components that have been inferred from studies taken at lower resolution.[21,22] However, for the present purpose, and taking into account the relatively low resolution under which these data were taken, a line-shape analysis with only two components is appropriate, since our main objective is the identification of the (7×7) phase and the precise position of the bulk line, in order to evaluate the position of the Fermi level in the gap in the two reconstructions.

The spectra from the 25%, 50%, and 75% mixtures can be well described by a straightforward superposition of the (7×7) and the Na(3×1) model functions. This is shown in the three center spectra of Fig. 5(a), where the complete model functions (i.e., sum of all surface and bulk contributions) rather than separate bulk and surface components are shown. The presence of the different fractions of Na(3×1) vs (7×7) reconstructions can actually be read off directly from the spectra, for example, from the second peak at low binding energy (the most intense one in the top spectrum), without recourse to line-shape analysis. The position of the bulk component in the Na(3×1) and the (7×7) spectra is indicated by the lines marked "*b*." The presence of the two clearly separated components, with their bulk lines shifted by about 0.6 eV, directly demonstrates the presence of a la-

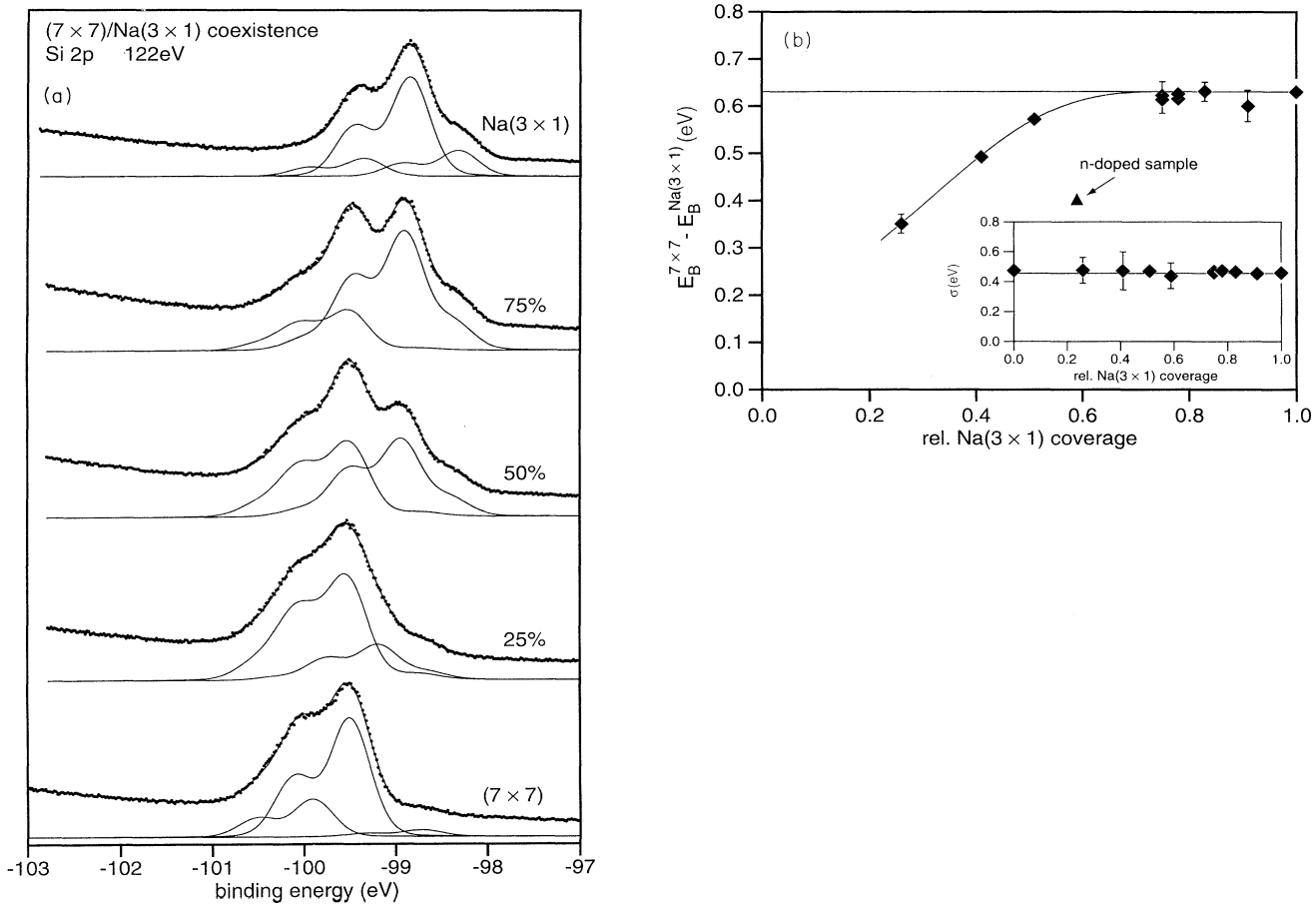

FIG. 5. (a) Si 2*p* spectra ranging from the pure Si(111)-(7×7) reconstruction (bottom) to the pure Si(111)-Na(3×1) reconstruction (top) with three intermediate stages of the phase transition from the (7×7) to the Na(3×1) reconstruction, corresponding to ≈25%, ≈50%, and ≈75% of Na(3×1) coverage. The components for a fit to the pure phases are given below the bottom and the top trace (solid lines). The three spectra in between are shown with the varying amount of (7×7) and Na(3×1) line shapes needed to describe the experimental data. The only fitting parameter needed to describe the spectra are the intensities of the Na(3×1) line shape and the (7×7) line shape, and the binding energy offset of the two contributions. (b) Binding energy of the Na(3×1) contribution to the spectra from the coexistence phase of the two surface reconstructions relative to the bulk component of the (7×7) contribution, which is fixed relative to the Fermi level. The inset shows the nonvarying Gaussian broadening of the components vs relative Na(3×1) coverage of the surface.

teral variation of the position of the Fermi-level in the band gap across the surface. Note that the only free parameter for the fitting of the spectra were the intensities of the (7×7) and the (3×1) bulk components (the intensity of the surface component of the respective phases is fixed relative to the bulk intensity) and the relative position of the (3×1) bulk component. This raises the question of the length scale for the changeover from the Na(3×1) to the (7×7) Fermi-level position. If a gradual changeover occurred, with a transition region on the order of 100 Å, one would expect a broadening of the distinctive features of both contributions, with a loss of the sharp features present in the data. Since this is not observed, we can deduce from the data that the changeover region must be much smaller than the average domain size, which as estimated from the STM images is less than 360 Å.

How can we understand such lateral variations of the Fermi level? Consider the situation of a bare surface first. Here, adatoms, defects, or surface states, all of which may carry charge, can produce a space-charge layer, which will extend laterally and into the bulk region, such that the opposite charge on the fixed ionized dopant atoms balances the charge. This leads to the well-known space-charge region with a characteristic decay length, which may be quite large for the low doping levels present in our samples, and a parabolic roll off of the potential with distance. The potential thus contains a term arising from the space-charge layer, and in addition a Coulomb term from the charged centers themselves. For low coverages, each center will be surrounded by a small region which is depleted of free carriers. As the coverage increases, the space-charge regions overlap, and then extend back into the crystal.[23] The critical coverage at which a uniform space-charge region is formed corresponds to a separation between adsorbates of roughly a Debye length. The Fermi-level positions for the set of data in Fig. 5(a) are shown in Fig. 5(b). Now for the *p*-type samples used here, the doping level of $(1-3)\times10^{15}$ cm^{-3} leads to a Debye length of about 1000 Å,[24] i.e., two orders of magnitude larger than would be expected from the occurrence of the sharp spectral features above. Since boron-doped surfaces are prepared by high-temperature annealing,[25,26] one might argue that boron out-diffusion has occurred, such that the doping level at the surface is much higher than in the bulk, as consequently the Debye length is much smaller. This possibility cannot be excluded; however, a *n*-doped sample, data for which are included in Fig. 5(b), shows a very similar behavior. Slight differences in the position of the Fermi level are readily explained by the higher misorientation and thus lower terrace width, leading to a smaller domain size of the difference reconstructions on the surface. (For the step structure of surfaces with higher misorientation cf. Ref. 14.) The Fermi level of this *n*-doped sample shows *p* doping at the surface, i.e., an inversion layer. Since the *n*-type sample is phosphorus-doped, boron segregation can be ruled out as reason for the Fermi-level position depicted in Fig. 5(b). We thus arrive at the conclusion, that the high-temperature treatment with sodium that is necessary to prepare the Na(3×1) reconstruction, induces a high level of *p*-type doping in the selvedge region. If we assume that the roll-over length of the Fermi level between the patches on Na(3×1) and (7×7) is about 10–20 Å, and, thus, the depletion region is of the same width, we arrive at a dopant concentration of roughly 5×10^{12} cm^{-2}.[24] This corresponds to about $\frac{1}{250}$th of a monolayer, which is below the natural defect density obtained by our sample preparation method.

The functional dependence of the lateral band offset in Fig. 5(b) demonstrates that the Na-induced doping of the surface is indeed very much localized at the surface. The lateral depletion length is too short to be imaged with the STM, but the depletion length below the surface is already considerably longer, since the difference in the Fermi levels saturates only at about 70% Na(3×1) coverage of the surface. If the high doping level would extend further into the bulk, one would expect saturation to occur earlier. Further evaluation of the depletion length perpendicular to the surface requires either the knowledge of the doping profile, which is not accessible by our experiments, or an assumption on the doping profile. Since its evaluation does not lead to a deeper insight into the nature of the surface reconstructions under investigation here, we will omit further analysis.

The nontrivial problem of the electrostatics of inhomogeneous Schottky barriers, which is equivalent to the problem of inhomogeneous Fermi-level positions, has been treated in detail by Tang and Freeouf[27] and Tung.[28] The first study discusses mainly the consequences of inhomogeneous Schottky barriers for transport measures, but while doing so, the Poisson equation has to be solved for the problem of inhomogeneous Fermi-level positions across the surface. The latter paper discusses the problem of the generation of inhomogeneous positions of the Fermi level at the surface by atomic defects and their measurement by surface sensitive methods such as Kelvin probe or core-level photoemission. Both papers do not deal directly with the problem discussed here. However, the number of theoretical papers discussing the problem of inhomogeneous positions of the Fermi level available is limited and these studies only give an impression on the problems and effects one encounters at surfaces with inhomogeneous Fermi-level positions. Figure 5 of Ref. 27, for example, demonstrates the depth dependence of the conduction-band minimum under a narrow strip of a low Schottky barrier on a *n*-type semiconductor, a situation comparable to our Fig. 5(b), which demonstrates the dependence of the Fermi-level position on the size of the Na(3×1) domains.

However, the present line of argument clearly demonstrates that the observed difference in Fermi-level position between the Na(3×1)- and the (7×7)-reconstructed domains implies a strong *p*-type doping of the surface generated by the Na treatment of the Si(111) surface used to obtain the Na-induced (3×1) reconstruction. Simple electrostatic considerations show that the high dopant concentration is consistent with the observed STM images of the sample, i.e., the dopant concentration is still lower than the defect density observed in the reconstructions, even if we assume δ doping of the surface layer itself.

Consider now the kinetics of the (7×7)→Na(3×1) phase transition. Figure 6 shows the intensity of the Na(3×1) contribution, normalized to the integrated intensity of the Si 2*p* emission as a function of Na flux (indicated by the dots, while a model to be described below is given by the solid line). Here, the Na flux is given in terms of units of evaporation time. There are two clearly separated regions in the functional dependence: the steep increase at the beginning of the (7×7)-Na(3×1) conversion and the sudden decrease in the conversion rate at a Na(3×1) coverage of the surface of 70–75 %. In the following section, we will describe the phase transition using a simple adsorption model; all assumptions made during the development of the model will be justified separately.

We assume that the adsorption rate $d\Theta/dt$ is given by

$$\frac{d\Theta}{dt}=S(\Theta)\frac{dN}{dt}\ , \tag{1}$$

where $S(\Theta)$ is the sticking probability for Na on the surface, which causes a local reconstruction, and $dN/dt=:\Phi$ denotes the rate of impinging Na atoms on the surface per unit area and second. The sticking probability is allowed to show a coverage dependence. The assumption underlying Eq. (1) is that there is no reevaporation of Na out of areas already converted to the Na(3×1) reconstruction. Rewriting this equation in terms of Na flux, with the assumption that each site that is already converted to the Na(3×1) reconstruction is blocked, i.e.,

$$S=(1-\Theta)\ , \tag{2}$$

one arrives at

$$\frac{d\Theta}{dt}=(1-\Theta)\Phi\ . \tag{3}$$

Since the normalized Na flux Φ is constant under our experimental conditions, a simple integration of this equation leads to

$$\Phi=1-e^{-\Phi t}\ . \tag{4}$$

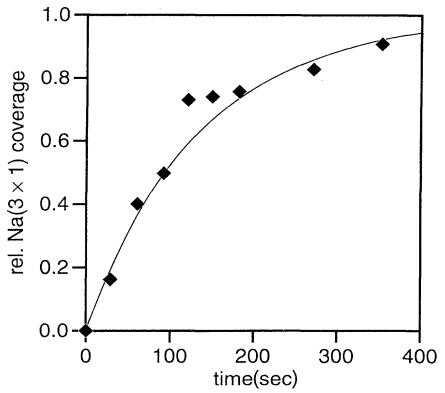

FIG. 6. Intensity of the Na(3×1) contribution to the Si 2*p* spectra normalized to the integrated intensity vs absolute flux of Na atoms impinging to the surface (dots). The solid line shows the Na(3×1) coverage of the surface as fitted to a simple model developed in the text.

A fit of this model to the experimental data leads to a flux constant Φ of $\Phi=(0.0075\pm0.0005)$ML(3×1)/s, i.e., if the sticking probability were unity, the Na flux would correspond to the growth of 1 ML of Na(3×1) reconstruction in (133±10) s, or using the Na density in the Na(3×1) reconstruction, the Na flux is at least 1 ML of Na in (400±30) s. The result of the fit to the model function is shown as a solid line in Fig. 6. The error given for the flux constant has been derived from a χ^2 analysis of the fit to the experimental data as a function of flux constant. This is in agreement with our calibration of the real Na flux in the room-temperature adsorption experiment, which leads to a flux of 1 ML of Na atoms in (210±30) s. Only if all Na atoms arriving at the 7×7-reconstructed areas of the surface were to be incorporated in the Na(3×1) reconstruction would the two different measurements of the flux have to yield identical results. The flux derived from the flux constant in Eqs. (3) and (4) thus leads to a lower limit for the Na flux, since it is not known, which fraction of Na atoms arriving at the (7×7) reconstruction act to revert it into the Na(3×1) reconstruction. However, by comparing the two flux measurements, it is found that actually about 50% of the Na atoms impinging on the 7×7-reconstructed areas will induce the Na(3×1) reconstruction under our experimental conditions. This is a surprising result, since STM data demonstrate that the phase transition exclusively proceeds through the step edges and then continues at the domain boundaries. A 50% efficiency for Na to change the surface reconstruction in the early stages of the phase transition implies that, even though the phase transition occurs at a temperature higher than the desorption temperature for Na from the Si(111)-(7×7) reconstruction, the time that the Na atoms stay on the surface is sufficient for 50% of them to diffuse to a step edge *and* induce the phase transition.

This simple model calculation, which reproduces the experimental data reasonably well, shows that the most important factor that determines the growth of the Na(3×1)-reconstructed domains, is the relative area of the remaining (7×7) reconstruction, i.e., in the rate of Na atoms arriving at the surface. At the growth rates used in our experiment, the formation rate of the Na(3×1) reconstruction is not diffusion limited. Different step densities might lead to different growth rates, since scanning-tunneling-microscopy experiments have shown that the phase transition from the (7×7) to the Na(3×1) reconstruction proceeds through the step edges of the surface, and transport of the Si atoms for the construction of the Na(3×1) over larger distances is necessary (see above). One could expect that the transport to the next step edge which acts as a sink for the excess Si atoms, is easier if the mean terrace width were smaller, i.e., the misorientation of the surface were larger. However, the overall dependence of the relative Na(3×1) coverages vs time at a given constant Na flux will not change. Other features that might influence the growth rate of the Na(3×1) patches on the (7×7) reconstruction, such as diffusion constants or kinetic restrictions, do not seem to be important at this level of precision, but certainly exert an influence on the functional

dependence of the Na(3×1) coverage vs time in the high coverage regime. In order to demonstrate the validity of this model for the transition from the (7×7) to the Na(3×1) reconstruction, we will have to justify the assumptions of the model: if the rate of conversion only depends on the relative amount of the (7×7) reconstruction on the surface, there should be a precursor state of Na on the (7×7) reconstruction at temperatures above the desorption temperature of Na from the Si(111)-(7×7) reconstruction. We are thus in a position to make certain predictions about the growth of Na(3×1) reconstruction.

(1) On quenched samples, Na must be present in a pre-Na(3×1) state or a kind of precursor state, which allows the Na atoms to diffuse on the surface before desorption.

(2) The Na has to adsorb on the 7×7 domains of the surface, not on the Na(3×1)-reconstructed domains.

(3) Reevaporation of Na from the Na(3×1)-reconstructed domains at the reaction temperature does not occur.

In the following section, we will focus on these three conditions. The last one is the easiest to justify, since the data shown from the pure Na(3×1) reconstruction are already from annealed samples. Furthermore, Olthoff, McKinnon, and Welland,[14] who have studied the desorption of Na from the Na(3×1) reconstruction, have kept their samples just below the temperature at which Na desorbs from the surface (which is at the upper end of the temperature window for the formation of this reconstruction) without noticing a degradation of the surface reconstruction. Thus the assumption leading to Eq. (1) is well satisfied. In order to check prediction 1 we have investigated the Na 2*p* core-level emission at very low coverages of the Na(3×1) reconstruction. This is shown in Fig. 7, which displays two Na 2*p* spectra of a sample that was converted to less than 5% of the Na(3×1) reconstruction. The top spectrum shows the sample directly after Na evaporation. The Na flux was switched off, and the sample was quenched to room temperature immediately thereafter. It was made sure that there was no Na flux present on the sample surface after the sample heating was switched off. The bottom spectrum shows the sample after an annealing step of 30 s at the reaction temperature. It is easily seen that this drastically alters the peak shape. A line-shape analysis (not shown here) reveals that the component at higher binding energy is reduced in intensity by the annealing procedure, while the intensity of the component at the lower binding energy is not changed within the error margins of line-shape analysis. This unchanged component corresponds to the typical Na 2*p* component in the Na(3×1) reconstruction, the line shape of which is discussed in detail elsewhere.[9] However, we take the presence of the second component in the spectra before annealing as evidence for the presence of Na in a precursor state on the surface.

The second contention is investigated by referring back to Fig. 4(b), which shows an STM image of a surface, nearly completely converted to the Na(3×1) reconstruction with atomic resolution. The main part of the image shows the remaining (7×7) reconstruction, while in the enter of the image, a Na(3×1)-reconstructed domain is visible. Here, the sample has been quenched to room temperature after the Na-adsorption. The assumption to be checked was that Na only exists on the (7×7)-reconstructed domains of such surfaces, and not on the Na(3×1) domains. It is easily seen that the Na(3×1) domain shows a nearly perfect reconstruction, while the (7×7) domain does not. There are a few clean (7×7)-unit cells, but most of them contain patches, which are imaged brighter, but do not show any internal structures. This brighter imaging of the structures might either be due to an electronic effect (increased density of states at the Fermi level) or to morphologic reasons [clusters on top of the (7×7) reconstruction]. On the basis of our present data, this cannot be decided, but it is likely that both processes contribute to the effect. First, there is no clear dependence of the imaging characteristics on the polarity of the voltage applied to the tunneling junction. Second, the two halves of the unit cell are not equally occupied by this bright imaged structure. The probability of finding the structures in the halves with the stacking fault is far larger than to find it in the ones without the stacking fault. This preferred site of the bright structures

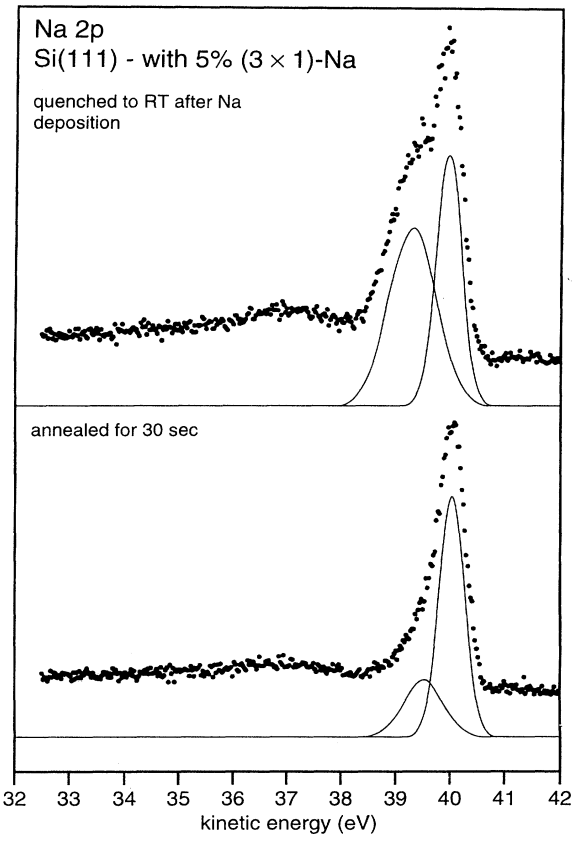

FIG. 7. Two Na 2*p* spectra taken from the same sample that is converted to the Na(3×1) reconstruction to an extent of less than 5%. The upper spectrum shows the sample, quenched to room temperature just after the Na flux was switched off. The bottom spectrum shows the same sample after 30 s of annealing at the reaction temperature. The intensity of component with the higher binding energy is drastically reduced by annealing, while the intensity of the other component remained constant.

is even more prominent in Fig. 4(a), where their distribution over nearly the entire (7×7) domain can be seen. The preferred orientation of the additional structures is seen in this image as a large-scale pattern, which covers nearly the entire domain. The observation of these structures is in agreement with the work of Jeon *et al.*[7] However, their composition is uncertain. From our photoemission data of the Na 2*p* core level it is clear that these structures must contain Na atoms. Whether Si atoms are involved in these structures is not certain, but likely, since for room-temperature adsorption of Na on the Si(111)-(7×7), a selective for Na adsorption on the two different halves of the unit cell is not observed.[9] Photoemission spectra of the Si 2*p* core level (not shown here) for the experiment presented in Fig. 7 are not helpful in this context, since the slight difference in the line shape before and after annealing might have two reasons: Si could be involved in these bright imaged structures, or the Na atoms adsorbed on the 7×7-domain changes core-level emission, which then would give rise to the change in the Si 2*p* line shape. Thus, the origin of these right imaged structures is not clear at present, but is of minor importance for the present discussion.

IV. CONCLUSIONS

Using a combination of photoemission and the scanning tunneling microscopy, we have shown that the alkali metal-induced structural phase transition from Si(111)-(7×7) to Si(111)-Na(3×1) proceeds exclusively through the step edges. The transition also involves a mass transport out of (7×7)-reconstructed domains for a conversion into the Na(3×1) domains. Using scanning tunneling microscopy, we find a strong anisotropy in the growth direction, which upon misorientation of the surface leads to the appearance of islands on larger domains of Na(3×1) reconstruction, which we have earlier attributed to the mass transport alone.[8] However, a careful investigation of the images at different Na(3×1) coverages of the surface has revealed that this structure results from both mass transport and the existence of preferred growth directions of the Na(3×1) reconstruction. In the coexistence regime of the two surface reconstructions, both constituents show only the properties of the pure surface reconstructions. Furthermore, we provide direct evidence for a lateral variation of the Fermi level across the surface of a semiconductor, which reaches up to (620±30) meV between the different reconstructions. The combination of core-level photoemission and the STM images of the coexisting surface reconstructions demonstrates that the Na treatment of the sample induces a high *p*-type doping level at the surface.

Beyond an assignment of the kinetics of the phase transition, a dynamical model of this phase transition describes the time dependence of the relative amount of Na(3×1)-reconstructed domains at a given Na flux. The only parameter, which influences the growth rate of the Na(3×1) domains is the amount of residual (7×7) reconstructed domains. The assumptions that lead to this simple model function were tested using independent experiments. This is a surprising and unexpected result, since the phase transition involves the transport of Si atoms across the remaining (7×7)-reconstructed domains, and one would therefore expect a behavior that is influenced mainly by the terrace width of the (7×7) reconstruction, which decreases with increasing Na(3×1) coverage.

ACKNOWLEDGMENTS

This work has been financed through BMFT under Grant No. 055EBFXB TP2. Dr. Wagner (Wacker Chemitronic GmbH) is acknowledged for kindly providing us with well-oriented silicon samples.

[1]E. H. Rhoderick and R. H. Williams, *Metal-Semiconductor Contacts* (Clarendon, Oxford, 1988).
[2]H. P. Bonzel, A. M. Bradshaw, and G. Ertl, in *Physics and Chemistry of Alkali Metal Adsorption* (Elsevier, Amsterdam, 1988), Vol. XX.
[3]H. Daimon and S. Ino, Surf. Sci. **164**, 320 (1985).
[4]M. Tikhov, L. Surnev, and M. Kiskinova, Phys. Rev. B **44**, 3222 (1991).
[5]R. Miranda, in *Physics and Chemistry of Alkali Metal Adsorption,* edited by H. P. Bonzel, A. M. Bradshaw, and G. Ertl (Elsevier, Amsterdam, 1989), p. 425.
[6]D. Jeon, T. Hashizume, T. Sakurai, and R. F. Willis, Phys. Rev. Lett. **69**, 1419 (1992).
[7]D.-R. Jeon, T. Hashizume, X. Wang, C. Bai, K. Motai, and T. Sakurai, Jpn. J. Appl. Phys. **31**, L501 (1992).
[8]J. J. Paggel, W. Theis, H. Haak, and K. Horn, J. Vac. Sci. Technol. B **11**, 1439 (1993).
[9]J. J. Paggel, G. Neuhold, H. Haak, and K. Horn (unpublished).
[10]K. J. Wan, X. F. Lin, and J. Nogami, Phys. Rev. B **46**, 13 635 (1992).
[11]J. M. Carpinelli and H. H. Weitering (unpublished).
[12]H. H. Weitering, N. J. DiNardo, R. Perez-Sandoz, J. Chen, and E. J. Mele, Phys. Rev. B **49**, 16 837 (1994).
[13]G. C. L. Wong, C. A. Lucas, D. Loretto, A. P. Payne, and P. H. Fuoss, Phys. Rev. Lett. **73**, 991 (1994).
[14]S. Olthoff, A. W. McKinnon, and M. E. Welland, Surf. Sci. **326**, 113 (1995).
[15]B. S. Swartzentruber, Y.-W. Mo, M. B. Webb, and M. G. Lagally, J. Vac. Sci. Technol. A **7**, 2901 (1989).
[16]H. Tokumoto, K. Miki, H. Murakami, and K. Kajimura, J. Vac. Sci. Technol. B **9**, 699 (1991).
[17]D. P. Woodruff and T. A. Delchar, *Modern Techniques of Surface Science* (Cambridge University Press, Cambridge, 1986).
[18]K. Takayanagi, Y. Tanishiro, S. Takahashi, and M. Takahashi, Surf. Sci. **164**, 367 (1985).
[19]K. Takayanagi, Y. Tanishiro, M. Takahashi, and S. Takahashi, J. Vac. Sci. Technol. A **3**, 1502 (1985).
[20]J. J. Paggel, W. Theis, K. Horn, C. Jung, C. Hellwig, and H. Petersen, Phys. Rev. B **50**, 18 686 (1994).
[21]F. J. Himpsel, P. Heimann, T.-C. Chiang, and D. Eastman, Phys. Rev. Lett. **45**, 1112 (1980).
[22]F. J. Himpsel, B. S. Meyerson, F. R. McFeely, J. F. Morar, A.

Taleb-Ibrahimi, and J. A. Yarmoff, in *Photoemission and Absorption Spectroscopy of Solids and Interfaces with Synchrotron Radiation,* edited by M. Campagna and R. Rosei (North-Holland, Varenna, 1988), p. 203.

[23]J. A. Stroscio and R. M. Feenstra, J. Vac. Sci. Technol. B **6**, 1472 (1988).

[24]S. M. Sze, *Physics of Semiconductor Devices* (Wiley, New York, 1981).

[25]E. Kaxiras, K. C. Pandey, F. J. Himpsel, and R. M. Tromp, Phys. Rev. B **41**, 1262 (1990).

[26]F. Thibauda, T. P. Roge, P. Mathiez, P. Dumas, and F. Salvan, Europhys. Lett. **25**, 353 (1994).

[27]J. Y.-F. Tang and J. L. Freeouf, J. Vac. Sci. Technol. B **2**, 459 (1984).

[28]R. T. Tung, Phys. Rev. B **45**, 13 509 (1992).

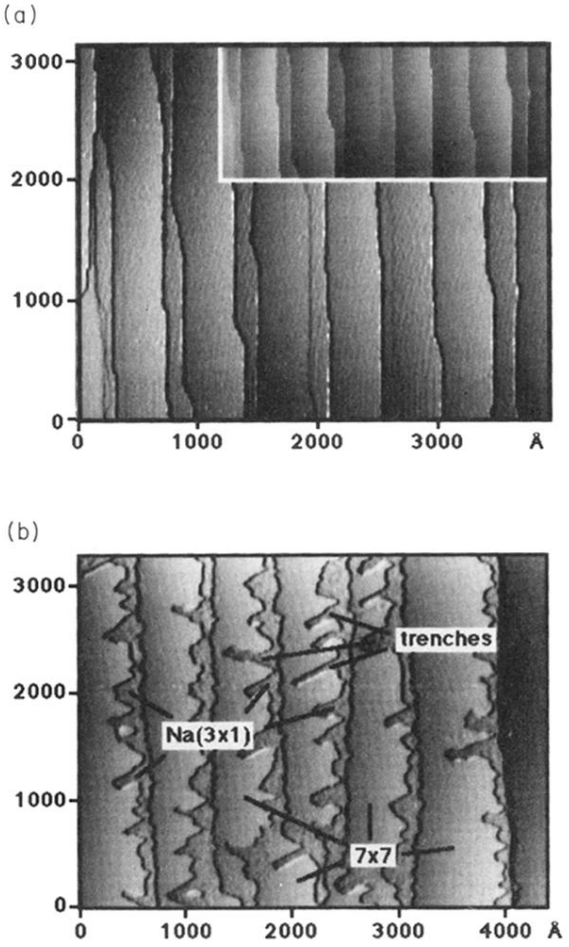

FIG. 1. Scanning-tunneling-microscopy images of (a) the clean Si(111)-(7×7) reconstructed surface with the typical straight step edges ($V_{\text{bias}}=1.5$ V, $I_t=900$ pA) and (b) the surface partially converted to the Na(3×1) reconstruction with "trenches" in the terraces extending into the terrace ($V_{\text{bias}}=1.8$ V, $I_t=1$ nA). The inset in (a) shows the bottom part of the image before picture processing. See text for details.

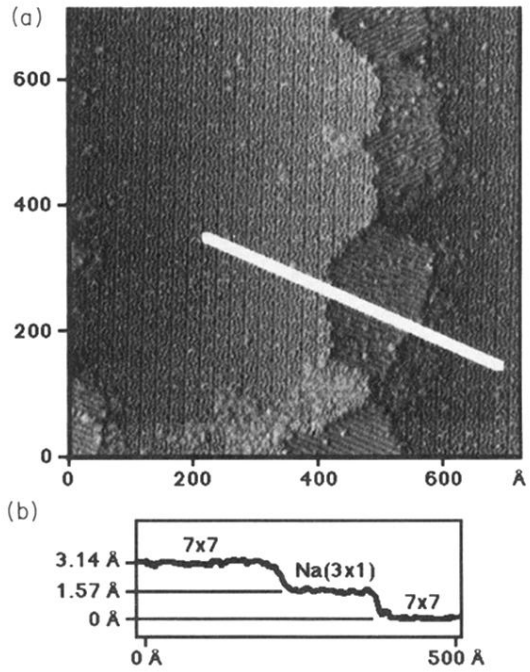

FIG. 2. Scanning-tunneling-microscopy image of the initial stage of the conversion of the (7×7) reconstruction into the Na(3×1) reconstructed surface with atomic resolution. Both types of domains do not show any sign of a lateral band bending across the terrace, which would be expected to result in a "bent terrace" ($V_{\text{bias}}=2.2$ V, $I_t=620$ pA).

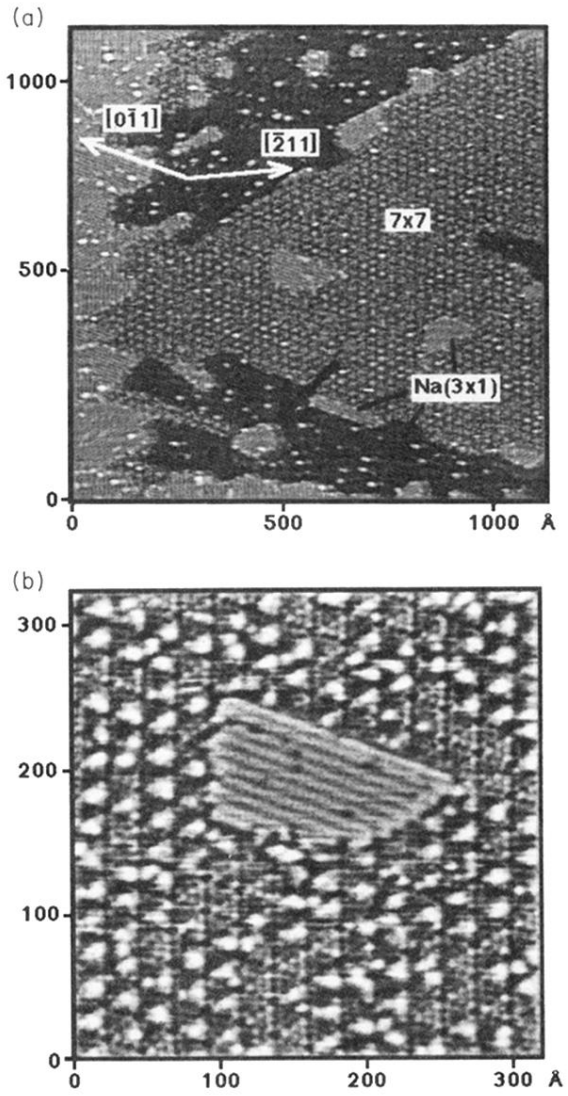

FIG. 3. (a) Large area scan of a nearly completely to the Na(3×1)-reconstruction converted surface ($V_{bias}=2.0$ V, $I_t=200$ pA). The large domain in the center of the image is (7×7) reconstructed, the surrounding domains are Na(3×1) reconstructed. For details see text. (b) Enlarged image of the island near the center of (a) on the (7×7) domain. The image shows the Na(3×1) reconstruction of the island, as well as the (7×7) reconstruction of the surrounding domain.

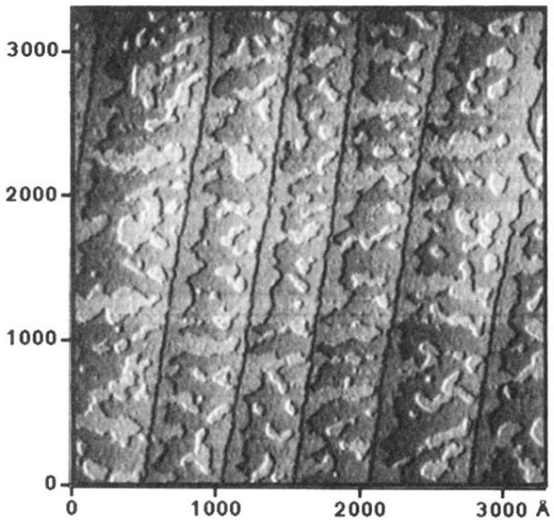

FIG. 4. STM image showing the step structure of a surface completely converted to the Na(3×1) reconstruction. All steps are 1 ML high. Note the existence of islands on larger terraces and the meandering step edges, which are never seen on the original (7×7)-reconstructed surface, which is the surface reconstruction used to prepare the Na(3×1) reconstruction on ($V_{\text{bias}}=1.5$ V, $I_t=460$ pA).